

Motion-enhancement to Echocardiography Segmentation via Inserting a Temporal Attention Module: An Efficient, Adaptable, and Scalable Approach

Md. Kamrul Hasan^a, Guang Yang^{b,c,d,e,1}, Choon Hwai Yap^{a,1,*}

^a*Department of Bioengineering, Imperial College London, London SW7 2AZ, UK*

^b*Bioengineering Department and Imperial-X, Imperial College London, London W12 7SL, UK*

^c*National Heart and Lung Institute, Imperial College London, London SW7 2AZ, UK*

^d*Cardiovascular Research Centre, Royal Brompton Hospital, London SW3 6NP, UK*

^e*School of Biomedical Engineering & Imaging Sciences, King's College London, London WC2R 2LS, UK*

Abstract

Cardiac anatomy segmentation is essential for clinical assessment of cardiac function and disease diagnosis to inform treatment and intervention. In performing segmentation, deep learning (DL) algorithms improved accuracy significantly compared to traditional image processing approaches. More recently, studies showed that enhancing DL segmentation with motion information can further improve it. A range of methods for injecting motion information has been proposed, but many of them increase the dimensionality of input images (which is computationally expensive) or have not used an optimal method to insert motion information, such as non-DL registration, non-attention-based networks, or single-headed attention. Here, we present a novel, computation-efficient alternative where a novel, scalable temporal attention module (TAM) extracts temporal feature interactions multiple times and where TAM has a multi-headed, KQV projection cross-attention architecture. The module can be seamlessly integrated into a wide range of existing CNN- or Transformer-based networks, providing novel flexibility for inclusion in future implementations. Extensive evaluations on different cardiac datasets—2D echocardiography (CAMUS) and 3D echocardiography (MITEA)—demonstrate the model’s effectiveness when integrated into well-established backbone networks like UNet, FCN8s, UNetR, SwinUNetR, and the recent I²UNet. We further find that the optimized TAM-enhanced FCN8s network performs well compared to contemporary alternatives. Our results confirm TAM’s robustness, scalability, and generalizability across diverse datasets and backbones.

Keywords: 2D/3D + time cardiac imaging, Deep learning, Motion-enhanced segmentation, Temporal attention module.

1. Introduction

Heart diseases are the most common cause of mortality, and echocardiography remains the most important imaging modality for evaluating heart diseases. Cardiac anatomy segmentation from echo images is an important tool for delineating cardiac chamber anatomy, which is important for quantifying anatomic parameters such as cardiac chamber shape, wall thicknesses, and chamber volumes, as well as quantifying cardiac function parameters, such as ejection fraction (EF), and stroke volume, ventricular and stroke volumes, atrial and ventricular remodeling [1, 2]. These quantifications are important for evaluating cardiac health to detect pathologic remodeling and inform treatment plans [3]. Early approaches to such segmentation were grounded in traditional image processing techniques, such as region growing [4], template matching [5], and level set [6]. While these methods had some success in specific cases, they often required manual intervention and lacked robustness when

applied to noisy or low-signal medical images [7]. For echocardiography, frequent low-quality images prevented reliable implementations, and segmentation remains a manual or semi-automatic task, which is time-consuming and a source of imprecision. Although clinical guidelines suggest that measurements should be repeated over three cardiac cycles for accuracy [8], this is often not done due to the time demands on clinicians, leading to imprecision in the cardiac measurements.

Advances in DL have enabled consistent, automatic segmentation with improved performance compared to traditional approaches [11–14]. Many convolutional neural networks (CNN)-based methods have reached promising performance and made notable progress [15], where the fully conventional networks (FCN8s, FCN16s, or FCN32s) [16] and the UNet [17] are two of the most popular CNN-based segmentation methods that have profound influences on subsequent works [7, 15]. Subsequently, Transformers were proposed for integration with CNNs to generate global feature extractions, overcome the limited spatial influence range of CNNs, and improve transferability to downstream tasks [18]. The Trans-UNet [19] was the first to tap into this potential by combining CNNs for low-level feature extraction with Transformers for high-level representations. Other successful models in cardiac image segmentation

*Corresponding author

Email addresses: k.hasan22@imperial.ac.uk OR
kamruleekuet@gmail.com (Md. Kamrul Hasan),
g.yang@imperial.ac.uk (Guang Yang), c.yap@imperial.ac.uk (Choon Hwai Yap)

¹Co-last senior authors.

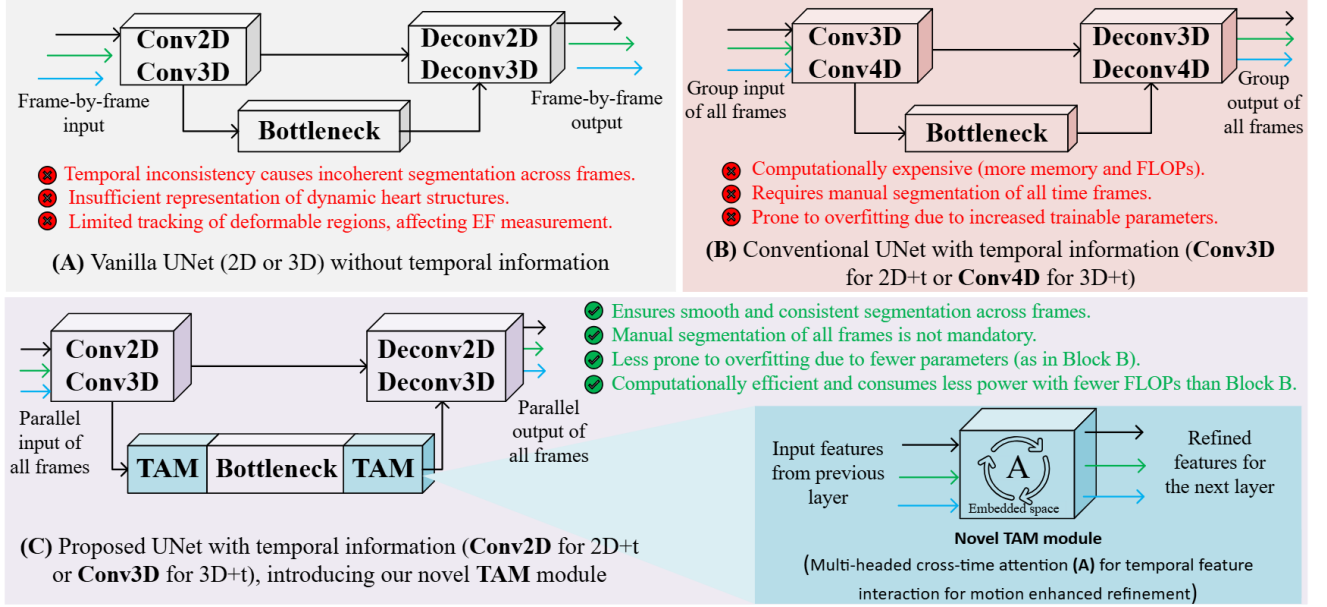


Figure 1: Illustration of the proposed temporal-aware segmentation model. (A) The baseline UNet (2D or 3D) processes inputs frame by frame, ignoring temporal information (time-independent). (B) A conventional temporal UNet incorporates time by using Conv3D for 2D+t [9] or Conv4D for 3D+t [10] data. (C) The proposed model improves temporal integration by combining Conv2D (for 2D+t) or Conv3D (for 3D+t) with a novel **Temporal Attention Module (TAM)**. The TAM employs multi-headed cross-time attention to refine motion features across frames, boosting segmentation quality while maintaining computational efficiency comparable to the model in (B) (Table 1).

Table 1: Computational overhead vs. segmentation quality in terms of Hausdorff Distance (HD) for various model configurations in Fig. 1. For 2D+t and 3D+t implementation, we consider only two frames ($t = 2$): ED and ES. Due to computational and data limitations, we only provide estimated FLOPs and parameter values for UNet4D (3D+t) to demonstrate its computational challenges.

Configurations	Images	Operations	Input tensor shape	Flops	Params	HD (mm)
Fig. 1 (A) UNet2D (frame-by-frame)	2D+t	2D	$1 \times 1 \times 256 \times 256$	$193G$	$31M$	5.11 ± 5.14
Fig. 1 (B) UNet3D (2D+t) [9]	2D+t	3D	$1 \times 1 \times 256 \times 256 \times t=2$	$1121G$	$87M$	5.65 ± 5.15
Fig. 1 (C) TAM-UNet2D (proposed)	2D+t	2D	$1 \times 1 \times 256 \times 256$	$228G$	$62M$	3.63 ± 2.69
Fig. 1 (A) UNet3D (frame-by-frame)	3D+t	3D	$1 \times 1 \times 128 \times 128 \times 128$	$7610G$	$90M$	12.26 ± 7.25
Fig. 1 (B) UNet4D (3D+t) [†] [10]	3D+t	4D	$1 \times 1 \times 128 \times 128 \times 128 \times t=2$	$30110G$	$260M$	–
Fig. 1 (C) TAM-UNet3D (proposed)	3D+t	3D	$1 \times 1 \times 128 \times 128 \times 128$	$7780G$	$171M$	10.48 ± 6.90

[†]We implemented a custom 4D network with the same layer count as a 3D network to directly compare computational overhead.

include LeViTUNet [20], CSwin-PNet [21], UNetR [22] and SwinUNetR [23].

In more recent implementations of DL segmentation networks, temporal motion features are used to improve performance. This approach is very logical and intuitive because, with the human eye, we often find it easier to distinguish cardiac structures from non-cardiac structures with videos rather than still images. Noise and signal losses are often impersistent across time, and incorporating motion features can reduce their effects to lead to better segmentation [24]. Several approaches to incorporating motion information have been attempted. A straightforward approach is to incorporate a time dimension and utilize a higher-dimensional CNN, such as through 3D (2D+t) or 4D (3D+t) networks [9, 10]. However, this approach has several limitations. First, it requires manual segmenting of many if not all frames [9], which is cumbersome, especially for 3D sequences. This is likely why no public 3D echo dataset with

complete temporal segmentation exists. Second, it significantly increases computational complexity (Table 1), particularly in 4D (3D+t) networks. With limited memory on GPU systems, they can be difficult to implement and slow. Thirdly, the large number of parameters involved in these models increases the risk of overfitting, particularly with smaller datasets. Hybrid approaches, which combine segmentation with temporal registration [9, 25] or Conv-LSTM [26], or which use a two-stage segmentation pipeline (e.g., teacher-student networks) [27, 28], have been proposed to generate performance enhancements. However, these methods can similarly be computationally expensive [9, 25, 26] and may still require substantial ground truth segmentations across the cardiac cycle [9, 25]. Further, their approach of incorporating motion features in segmentation is likely not optimal: non-DL registrations are known to be imperfect [25], while DL registrations are likely to be improvable with attention mechanisms [9, 26]. Finally, to date,

all motion-informed DL segmentation networks are proposed as standalone frameworks, including those that utilize temporal attention [27, 29], and their motion enhancement mechanisms are not easily extracted for integration into another network or a future network.

To address these issues, we propose a novel approach to incorporating motion features into a segmentation network in a computationally efficient way. We propose a temporal attention module (TAM) that can be integrated into both CNN- and Transformer-based architectures to enhance their ability to learn temporal features without excessive computational overhead (Fig. 1 (C) and Table 1). TAM’s lightweight design ensures easy integration into a network and ensures computational efficiency. The specific key contributions of our work are:

- **Novel Temporal Attention Mechanism for Segmentation:** We present a new Temporal Attention Module (TAM), a multi-headed, temporal cross-time attention mechanism based on KQV projection, that enables the network to effectively capture dynamic changes across temporal frames for motion-enhanced cardiac anatomy segmentation.
- **Flexible Integration into a range of Segmentation Networks:** TAM can be flexibly, plug-and-play integrated into a range of established backbone segmentation architectures, including UNet, FCN8s, UNetR, SwinUNetR, and I²UNet [30], to arm them with motion-awareness. This offers a simple and elegant approach to implementing motion awareness in future networks.
- **Consistent Performance Across Multiple Settings:** Through experiments on multiple cardiac datasets (2D and 3D), we demonstrate that TAM is generalizable across image type and quality and is scalable from 2D to 3D; through experiments across various backbone segmentation architectures, we show that TAM consistently improves segmentation performance and is thus highly adaptable; through flops estimations, we show that TAM adds minimal computational overhead to the network it enhances, and is more computationally efficient than adding time as an extra image dimension.

2. Related Works

2.1. Motion excluded segmentation models

Since the introduction of the UNet design [17], several CNN-based approaches [31–34] have extended the standard UNet architecture for various medical image segmentation tasks. For example, the authors in [31] introduce a generalized segmentation framework named nnUNet that automatically configures the architecture to extract features at multiple scales. Further, several efforts in the literature have been made to encode holistic contextual information within CNN-based frameworks using, e.g., image pyramids [35], large kernels [36], dilated convolution [37], and deformable convolution [38].

More recent segmentation networks, however, have mostly incorporated transformers to enhance effectiveness. Many intend to combine the transformer’s ability to capture global features with CNN’s ability to capture local features. For example, Zhou et al. [39] introduced nnFormer, a 3D transformer for volumetric medical image segmentation, which has an interesting interleaved architecture of alternative convolution blocks and transformer blocks, which, when combined with skipped attention rather than skipped connections, achieves both local and global volume-based self-attention. Zhao et al. [40] proposed a semi-supervised echocardiography segmentation method using a boundary attention transformer (BATNet) to capture spatial information and a multi-scale, semi-supervised model (semi-BATNet) to enforce boundary feature consistency. Zhang et al. [41] proposed BSANet for cardiac MRI segmentation, using a multi-scale boundary-aware module that improves edge extraction and a scale-aggregation transformer module to retain features of various scales for enhanced performance. Shaker et al. [42] proposed UNETR++, a 3D medical image segmentation approach that balances segmentation quality and computational efficiency. The key innovation is the efficient paired attention (EPA) block, which uses two interdependent branches based on spatial and channel attention to improve the learning of discriminative features. Qin et al. [43] introduced an uncertainty-based region clipping algorithm for semi-supervised medical image segmentation. A module computes the uncertainty of two sub-networks predictions using Monte Carlo Dropout, while another module generates new samples by masking low-confidence pixels based on uncertainty. Li et al. [44] introduced TPAFNet, a multi-scale 3D medical image segmentation network combining CNN and transformer. This uses a TPAF module that extracts channel weights through convolution for integration with the Transformer, an atrous convolution to send multi-scale information to the Transformer, and a voxel-wise classifier for deep supervision.

Although these works offered effective and innovative advancements in segmentation, a general limitation is their need for more consideration of temporal information. They focus solely on spatial features, treating each image frame independently without accounting for temporal relationships between frames. Consequently, these models may struggle with consistency over time and experience artifacts or discontinuity between successive frames [9, 45]. There is a missed opportunity for using neighboring time frames to reduce noise and enhance signals in the current frame [27]. These are important for echocardiography because echo images have significant noise and signal losses and because the heart undergoes substantial cyclic motion, and accurate assessment of such motion is important for clinical evaluation.

2.2. Motion-enhanced segmentation models

Several previous studies have used temporal motion information to enhance segmentation networks and reported the benefits of this approach.

The most straightforward approach is proposed by Myronenko et al. [10], who utilized a 4D CNN for segmenting ECG-gated cardiac CT. The network has a loss function that supports

training with sparse labeling, with labels at only a few time frames. They showed that this produced superior smoothness but comparable DICE as a 3D segmentation network. Xue et al. [25] proposed an echocardiography segmentation method that effectively utilizes motion information from optical flow image registration motion fields, which improved segmentation accuracy. A shared feature extractor was used for the segmentation and optical flow sub-tasks to enable efficient information exchange. At the same time, an orientation congruency constraint promotes consistency between optical flow fields of successive frames. Wei et al. [9] proposed the CLAS network, which concurrently predicts segmentation masks and bi-directional (forward and backward in time) motion fields. A common encoder but separate decoders were used for the two predictions, and loss functions were designed to enforce the consistency of the two outputs with each other and the images. The authors proposed a multi-task version, MCLAS Wei et al. [28], that performed echo view classification and direct ejection fraction prediction using the CLAS backbone. Maani et al. [45] introduced SimLVSeg, a novel network for left ventricle segmentation from echocardiogram videos with sparse annotations to address the difficulty of obtaining annotation ground truths. First, a self-supervised network that recovers intentionally masked temporal frames is pre-trained. The encoder of this network is then used to train the LV segmentation network using sparse annotations for weakly supervised training. In the process, the understanding of temporal sequences of frames is passed on to the segmentation network. Li et al. [26] proposed a recurrent aggregation learning method for multi-view echocardiographic sequence segmentation. It uses pyramid ConvBlocks for efficient feature extraction and hierarchical ConvLSTMs to capture temporal evolution. A double-branch aggregation mechanism is introduced, where segmentation and classification branches enhance each other.

Despite successfully using temporal information to enhance segmentation, they use complex and resource-intensive approaches to inject temporal information into their networks. The time dimension increases the image dimension, requiring the input of the entire or most of the image sequence, which substantially increases memory requirements and computational burden. Some of them involve additional classification or registration subtasks, resulting in added complexity and a larger number of parameters to be trained, which increases the risk of overfitting. The use of optical flow, a traditional image registration approach, may further be a limitation, as deep learning approaches have better performance. Similarly, network-based registration may improve by using transformers. To address these limitations, we seek to develop an alternative approach that is structurally simple and computationally inexpensive and does not require inputs of an excessive number of time frames for effective extraction of motion information.

Recent work has also proposed using attention mechanisms to extract temporal information for segmentation. For example, Ahn et al. [29] proposed a multi-frame attention network to improve left ventricle segmentation in 3D echocardiography. The approach incorporates a multi-frame co-attention mechanism that utilizes correlated spatiotemporal features from im-

ages of different time frames to enhance segmentation performance. Wu et al. [27] proposed a network that takes in three consecutive echocardiography image time frames for segmentation, where cross-attention between neighboring time frames is used to extract features and enhance skipped connections to enhance segmentation performance. They propose that this can address the challenges of speckle noise, irregular heart motion, and limited training data. These are excellent, innovative ideas. However, the proposed approaches for motion-informed enhancement are standalone frameworks and cannot be easily extracted for integration into another or future network. Here, we investigate an alternative attention mechanism, based on the multi-headed KQV projection, and we seek an alternative approach to enable more flexible incorporation into other networks.

3. Methodology and Materials

3.1. Proposed motion-enhanced segmentation

We propose to extract and utilize temporal features in segmentation networks via a plug-and-play temporal attention module (TAM) that can be seamlessly incorporated into a range of backbone segmentation algorithms, including UNet, FCN8s, UNetR, SwinUNetR, and I²UNet [30]. Adding our novel TAM, as shown in Fig. 2, enables the network to explicitly model these temporal relationships, allowing it to segment dynamically changing regions accurately. TAM identifies which frames and spatial regions are most relevant for segmenting the target frame, ensuring the network focuses on meaningful temporal variations. TAM uses its temporal awareness to fuse features across time by aggregating contributions from temporal neighbors and emphasizing regions with temporal coherence. This step ensures robust feature refinement for dynamic regions, critical for segmenting motion-sensitive areas. The gating mechanism in TAM suppresses irrelevant or noisy temporal information, improving the segmentation quality in loud environments (e.g., due to motion artifacts or low contrast in cardiac imaging).

In the next sections, we first explain the CNN, Transformer, or CNN+Transformer hybrid backbone segmentation networks to which we tested the addition of TAM and then the TAM module.

3.1.1. Backbone segmentation models

Fig. 2 presents our proposed motion-aware segmentation framework. Our proposed TAM module is explained in Fig. 2 (C) and explained in more detail below. It serves as a plug-and-play solution for motion-aware enhancement to address the limitations of networks without motion-awareness. UNetR and UNet are foundational networks that lacked motion awareness, and Fig. 2 (A) and (B) demonstrate how TAM can be inserted into these networks for enhancement, forming the TAM-UNetR and TAM-UNet. The idea is for TAM to guide a selective focus on motion-coherent features across time frames while suppressing irrelevant or noisy information to improve segmentation performance, especially in noisy images with poor signals

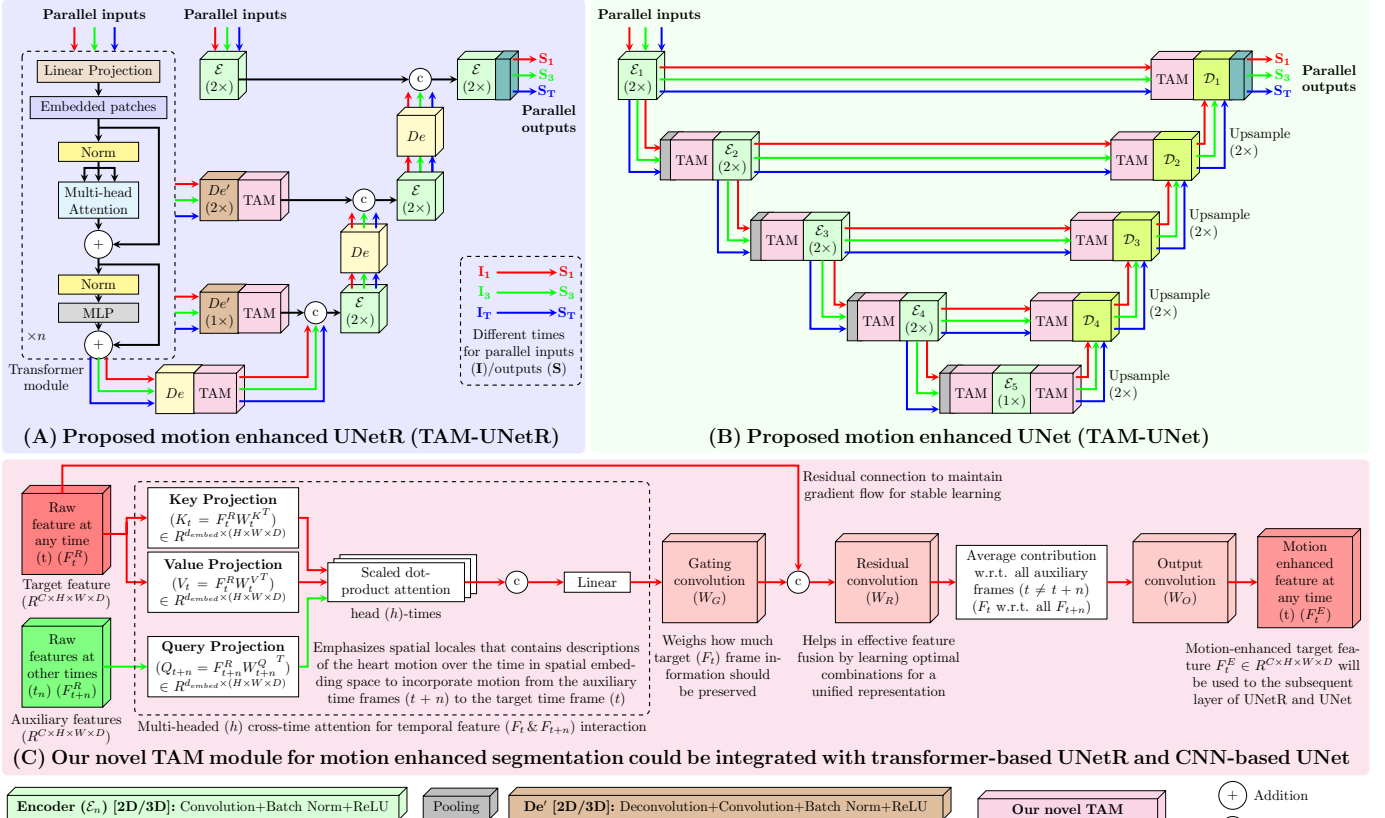


Figure 2: The proposed model enhances temporal integration by coupling our novel **TAM** with either a Conv2D (for 2D+t) or Conv3D (for 3D+t) network. In (A), TAM is integrated into the transformer-based UNetR model, while (B) demonstrates its integration with the CNN-based UNet. The TAM (as shown in (C)) leverages multi-headed cross-time attention to refine motion features across frames, improving segmentation quality without the computational overhead typically incurred by adding extra dimensions to the input tensors [9, 10] (as shown in Fig. 1 and Table 1).

like echocardiography and where images have complex motions such as that of the heart.

To implement the insertion, the networks must first be modified to simultaneously input several (e.g., 2-5) time frames. This increases the dimension of the input images but involves only a limited increase in input data size. In both UNetR and UNet, several TAM modules will be strategically placed at various encoder or decoder layers. The possible insertion locations are shown in Fig. 2 (A) and (B), and the exact configuration of insertion locations should be determined by optimization studies, as demonstrated by our ablation study in Section 4.1. Where it is inserted, TAM refines the feature maps to guide a focus on coherent motion dynamics.

3.1.2. Temporal attention module (TAM)

As shown in Fig. 2C, TAM is integrated between two layers of the model. TAM receives T number of temporal feature maps $\{F_1, F_2, \dots, F_T\} \in \mathbb{R}^{C \times H \times W \times D}$ ($t \forall T$) from the previous layer and facilitates temporal feature interaction (in between F_{t-i} and F_{t+j} , where $i \neq j$) in the embedded space to refine the input features $\{F_1^{\text{refined}}, F_2^{\text{refined}}, \dots, F_T^{\text{refined}}\} \in \mathbb{R}^{C \times H \times W \times D}$ for the subsequent layer. This highlights cardiac regions and frames that contribute most to the refined representation, providing insights into the motion refinement process. Algorithm 1 explains

step-by-step procedures for such motion-enhanced feature refinements, and the following paragraphs explain the details of operations and rationale.

Linear Transformations: In the first step, linear transformations are applied to each feature map, F_t ($t \forall T$), using trainable weight matrices (W_q, W_k, W_v) and biases (b_q, b_k, b_v), to form the Query (Q_t), Key (K_t), and Value (V_t) components of the Transformer.

$$\begin{aligned} Q_t &= F_t W_q^T + b_q, \\ K_t &= F_t W_k^T + b_k, \\ V_t &= F_t W_v^T + b_v, \end{aligned}$$

where K and V encode information in the current frame, and Q represents the information being sought for from other frames. Then, the embeddings are divided into H_{heads} subspaces to allow the model to capture diverse patterns of temporal relevance across different spatial regions, for example, subtle versus significant motions and simple versus complex motions. This also helps to capture richer spatial-temporal relationships across different subspaces.

Multi-head Cross-time Attention: The cross-time attention matrix (A) is computed from K , V , and Q to capture relation-

Algorithm 1: Multi-headed cross-time attention algorithm of our novel TAM.

Input: A set of feature maps $\{F_1, F_2, \dots, F_T\} \in \mathbb{R}^{C \times H \times W \times D}$, embedding dimension d_{embed} , attention head numbers H_{heads} .

Output: A set of refined motion-enhanced feature maps $\{F_1^{\text{refined}}, F_2^{\text{refined}}, \dots, F_T^{\text{refined}}\} \in \mathbb{R}^{C \times H \times W \times D}$.

1 Compute query, key, and value projections:

$$Q_t = F_t W_q^T + b_q, \quad K_t = F_t W_k^T + b_k, \quad \text{and} \quad V_t = F_t W_v^T + b_v, \quad \text{where } Q_t, K_t, V_t \in \mathbb{R}^{d_{\text{embed}} \times (H \times W \times D)}$$

2 Split Q_t, K_t, V_t into multiple heads H_{heads} :

$$Q_t^h \in \mathbb{R}^{\frac{d_{\text{embed}}}{H_{\text{heads}}} \times (H \times W \times D)}, \quad K_t^h \in \mathbb{R}^{\frac{d_{\text{embed}}}{H_{\text{heads}}} \times (H \times W \times D)}, \quad \text{and} \quad V_t^h \in \mathbb{R}^{\frac{d_{\text{embed}}}{H_{\text{heads}}} \times (H \times W \times D)}, \quad \forall h \in \{1, 2, \dots, H_{\text{heads}}\}$$

3 Compute the multi-head cross-attention for the i^{th} time with respect to j^{th} time ($i \neq j$) across all heads h :

$$A_{i \leftarrow j}^h = \text{softmax} \left(\frac{Q_i^h K_j^{h \top}}{\sqrt{d_{\text{embed}} / H_{\text{heads}}}} \right) V_j^h, \quad i, j \forall T, \quad A_{i \leftarrow j}^{\text{multi-head}} = \text{Concat}(A_{i \leftarrow j}^1, A_{i \leftarrow j}^2, \dots, A_{i \leftarrow j}^{H_{\text{heads}}})$$

4 Apply a gating operation using a gating convolution (W_G):

$$G_{i \leftarrow j} = W_G * A_{i \leftarrow j}^{\text{multi-head}}, \quad A_{i \leftarrow j}^{\text{gated}} = A_{i \leftarrow j}^{\text{multi-head}} \odot G_{i \leftarrow j}$$

5 Apply residual concatenation and convolution (W_R):

$$F_i^{\text{combined}} = \text{Concat}(F_i, A_{i \leftarrow j}^{\text{gated}}), \quad F_i^R = W_R * F_i^{\text{combined}}$$

6 Aggregate the results by averaging across all contributing frames $j \neq i$ and apply the output convolution (W_O):

$$F_i^{\text{Avg}} = \frac{1}{T-1} \sum_{j \neq i}^T F_j^R, \quad F_i^{\text{refined}} = W_O * F_i^{\text{Avg}}$$

7 Return refined motion-enhanced feature maps $\{F_1^{\text{refined}}, F_2^{\text{refined}}, \dots, F_T^{\text{refined}}\} \in \mathbb{R}^{C \times H \times W \times D}$

ships between the target frame i and all other frames $j \neq i$, expressed as:

$$A_{i \leftarrow j}^h = \text{softmax} \left(\frac{Q_i^h K_j^{h \top}}{\sqrt{d_{\text{embed}} / H_{\text{heads}}}} \right) V_j^h, \quad i, j \forall T$$

$$A_{i \leftarrow j}^{\text{multi-head}} = \text{Concat}(A_{i \leftarrow j}^1, A_{i \leftarrow j}^2, \dots, A_{i \leftarrow j}^{H_{\text{heads}}})$$

A is scaled by $\sqrt{d_{\text{embed}} / H_{\text{heads}}}$ to stabilize gradient updates during training and to prevent dominance of large values in dot products. The softmax normalizes attention scores across all spatial-temporal positions that ensure that attention weights prioritize the most relevant temporal and spatial regions while suppressing irrelevant information. Subsequently, the concatenation of A from various heads ensures that diverse attention outputs from all heads are merged into a single comprehensive representation. The output preserves the embedding dimension d_{embed} , ensuring compatibility with downstream operations. Consolidating multi-head attention outputs ensures the model captures interdependencies crucial for motion refinement.

Gated Cross-time Attention: To address the inherent appearance variations between input pairs and challenges such as signal losses and background noise, information from different

input frames are weighted differently, which is more effective than treating all co-attention information equally [46]. A self-gating mechanism is thus introduced to assign a co-attention confidence score to each attention summary to more effectively highlight motion-relevant regions and deemphasize irrelevant regions. The gating mechanism is defined using the gating convolution (W_G) and bias (b_G), as follows:

$$G_{i \leftarrow j} = \sigma(W_G * A_{i \leftarrow j}^{\text{multi-head}} + b_G), \quad A_{i \leftarrow j}^{\text{gated}} = A_{i \leftarrow j}^{\text{multi-head}} \odot G_{i \leftarrow j}$$

where the scaling using the logistic sigmoid activation function (σ) converts gating values to be between 0 and 1, enabling fine-grained control over each spatial-temporal region's contribution. The gate determines the extent to which information from the reference frame is preserved and learned automatically. Once the gate confidences are computed, the attention summaries are updated using channel-wise Hadamard products (\odot) between $A_{i \leftarrow j}^{\text{multi-head}}$ and $G_{i \leftarrow j}$. These operations collectively form a gated co-attention framework that modulates spatial and temporal information.

Combining Attention with Target Features: Next, we concatenate original feature maps with the gated attention output to obtain F^{combined} . This retains the foundational spatial-temporal

structure while enhancing it with refined temporal relationships, emphasizing specific features and locations. This is formulated as:

$$F_i^{\text{combined}} = \text{Concat}(F_i, A_{i \rightarrow j}^{\text{gated}}), F_i^R = \text{ReLU}(\text{BN}(W_R * F_i^{\text{combined}}))$$

where W_R is a convolution operation that aggregates local spatial information and introduces non-linearity to enable further refinement of the feature representation. BN is the batch normalization that stabilizes training by normalizing feature distributions across the batch, ensuring faster convergence and better generalization. The ReLU activation further introduces non-linearity, which is critical for modeling complex spatial-temporal patterns.

Temporal Aggregation: Motion features across all frames $j \neq i$ are then aggregated for temporal coherence. This is formulated as:

$$F_i^{\text{Avg}} = \frac{1}{T-1} \sum_{j \neq i}^T F_j^R, \quad F_i^{\text{refined}} = W_O * F_i^{\text{Avg}}$$

where T is the number of frames inputted, which is an optimizable hyperparameter in TAM (see ablation in section 4.1), W_O is the output convolution that aggregates temporal information into a compact representation for the current frame, reducing dimensionality while preserving motion-relevant details. Excluding frame i prevents self-referencing while ensuring that inter-frame dependencies are captured in TAM. The final refined feature maps, F_i^{refined} , are now enhanced with temporal motion information, making them better suited for downstream tasks.

Loss Function: Aligned with recent literature [39, 42, 47], our loss function combines the widely used Dice coefficient and cross-entropy losses, harnessing the complementary advantages of both. This combined loss (\mathcal{L}) is formulated as follows:

$$\mathcal{L}(S_T, S_P) = 1 - \sum_{i \in C} \left(\frac{2 \cdot |S_T^i \cap S_P^i|}{|S_T^i| + |S_P^i|} + \sum_{x \in N} S_T^i(x) \log S_P^i(x) \right) \quad (1)$$

where C is the number of anatomic organs and N is the number of elements in true and predicted anatomical masks (S_T and S_P).

3.2. Datasets and Implementation

3.2.1. 2D echocardiography (CAMUS)

This adult dataset [11] includes 500 patients with apical 2-chamber and 4-chamber views. It is acquired from GE Vivid E95 ultrasound scanners (GE Vingmed Ultrasound, Horten, Norway) with a GE M5S probe, with a pixel resolution of $0.154\text{mm} \times 0.154\text{mm}$. Further descriptions of the CAMUS dataset can be found in [11]. Out of 500 patients, 50 are selected for testing data, and the remaining patients are used for training and validation data.

3.2.2. 3D echocardiography (MITEA)

We utilize the MITEA dataset for training and testing, a 3D adult echo comprising 134 human patients with 268 sample acquisitions at the end-diastolic (ED) and end-systolic (ES) [13], which gives 536 3D image volumes (details in [13]). The volumes are provided with anatomical segmentation masks. The sample distribution for training-validation/testing of seven different classes is as follows: 328 (304/24) healthy, 56 (48/8) with left ventricular hypertrophy, 48 (36/12) with cardiac amyloidosis, 40 (32/8) with aortic regurgitation, 32 (28/4) with hypertrophic cardiomyopathy, 24 (20/4) with dilated cardiomyopathy, and 8 (4/4) with heart transplant recipients.

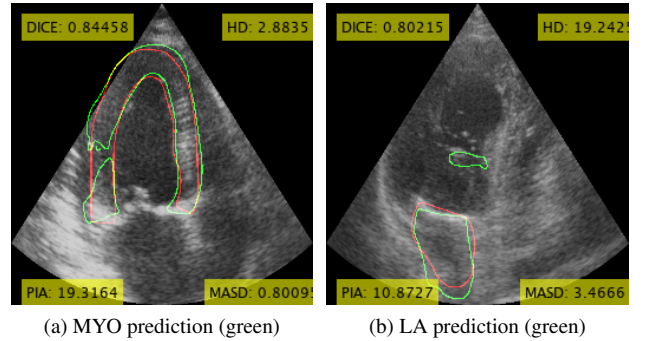


Figure 3: While DICE displays favorable results for both predictions, it disregards the anatomical plausibility and penalizes significantly in a low margin. In contrast, our PIA measure shows that (a) has a 19.32% disconnected region and (b) has a 10.87% island.

3.2.3. Training protocol and evaluation

We evaluate the results using the dice similarity coefficient (DSC) for overlapping precision, the Hausdorff distance (HD) for border irregularity, and the mean average surface distance (MASD) for the average distance between the predicted and ground truth masks that assesses the spatial dissimilarity by calculating the average distance between corresponding points on surfaces, as defined in 2 for the true and predicted masks ($S_T \& S_P \in \mathcal{R}^N$) for N -dimension.

$$\begin{aligned} \text{DSC}(S_T^C, S_P^C) &= \frac{2 \cdot |S_T^C \cap S_P^C|}{|S_T^C| + |S_P^C|}, \\ \text{HD}(S_T^C, S_P^C) &= \max \left\{ \max_{a \in S_T^C} \min_{b \in S_P^C} d(a, b), \max_{b \in S_P^C} \min_{a \in S_T^C} d(b, a) \right\}, \\ \text{MASD}(S_T^C, S_P^C) &= \frac{1}{|S_T^C| + |S_P^C|} \left(\sum_{a \in S_T^C} \min_{b \in S_P^C} d(a, b) + \sum_{b \in S_P^C} \min_{a \in S_T^C} d(b, a) \right), \end{aligned} \quad (2)$$

where C is the number of anatomic organs. $d(a, b)$ is the Euclidean distance between points a and b , and $\min_{a \in S_P^C} d(a, b)$ represents the minimum distance from a point a on surface S_T^C to the closest point b on surface S_P^C , and vice versa for $\min_{a \in S_T^C} d(b, a)$.

Table 2: Segmentation results on the 2D CAMUS dataset [11] using various configurations of the TAM-UNet2D alongside two baseline models. We used ED-ES frames, and the number of heads was 8 in this experiment.

Configurations (C)		DSC (\uparrow)	HD (\downarrow)	MASD (\downarrow)	PIA (\downarrow)	FLOPs (\downarrow)	Params (\downarrow)
UNet2D (without motion)	C1	0.913	5.11 mm	1.13 mm	2.05 %	193 G	31 M
UNet3D (2D+t) (with motion)	C2	0.915	5.65 mm	1.15 mm	2.52 %	1121 G	87 M
Different configurations of our motion-enhanced TAM-UNet2D (Fig. 2)							
TAM after \mathcal{E}_5	C3	0.921	3.90 mm	0.986 mm	1.18 %	221 G	58 M
TAM after $\mathcal{E}_4 \& \mathcal{E}_5$	C4	0.922	3.63 mm	0.961 mm	1.79 %	228 G	62 M
TAM after $\mathcal{E}_3, \mathcal{E}_4 \& \mathcal{E}_5$	C5	0.923	3.51 mm	0.954 mm	2.92 %	237 G	66 M
TAM after $\mathcal{E}_5 +$ before \mathcal{D}_4	C6	0.923	3.68 mm	0.952 mm	2.08 %	253 G	65 M
TAM after $\mathcal{E}_5 +$ before $\mathcal{D}_3 \& \mathcal{D}_4$	C7	0.923	4.05 mm	0.966 mm	1.82 %	316 G	66 M
TAM after $\mathcal{E}_4 \& \mathcal{E}_5 +$ before \mathcal{D}_4	C8	0.923	3.55 mm	0.957 mm	4.13 %	270 G	66 M
TAM after $\mathcal{E}_4 \& \mathcal{E}_5 +$ before $\mathcal{D}_3 \& \mathcal{D}_4$	C9	0.921	4.04 mm	0.980 mm	2.17 %	332 G	68 M
TAM after $\mathcal{E}_3, \mathcal{E}_4 \& \mathcal{E}_5 +$ before \mathcal{D}_4	C10	0.922	3.79 mm	0.969 mm	3.50 %	260 G	67 M
TAM after $\mathcal{E}_3, \mathcal{E}_4 \& \mathcal{E}_5 +$ before $\mathcal{D}_3 \& \mathcal{D}_4$	C11	0.920	3.80 mm	0.977 mm	2.32 %	323 G	68 M

In addition, we evaluate the propensity of the network to generate erroneous small disconnected segmentation islands that are detached from the main segmentation mass (Fig. 3B), and to erroneously divide the segmentation into disconnected large masses (Fig. 3A). To evaluate this, we calculate the percentage of the total segmentation area accounted for by such “island areas”, defined as any segmentation mass that is not the largest and that is disconnected from the largest mass. PIA measures anatomical plausibility, using the predicted mask alone, and does not require the ground truth mask. It is formulated based on the principle that the segmented myocardial or luminal areas should be a single connected mass.

$$\text{PIA} = \frac{1}{C} \sum_{c=1}^C \left(\frac{\sum_{r=1}^{R_c} A_{cr} - A_{c,\text{largest}}}{A_{c,\text{largest}}} \times 100 \right), \quad (3)$$

where C and R_c are the number of anatomic organs in S_P and the number of connected components in the c^{th} anatomical organ in S_P . A_{cr} is the area of the r^{th} connected component of any organ $c \forall C$, and $A_{c,\text{largest}} = \max(A_{c1}, A_{c2}, \dots, A_{cR_c})$.

4. Experimental Results

4.1. TAM design and ablation

To optimize the multi-headed TAM design, we systematically fine-tuned key hyperparameters, including the number of attention heads, the number of time frames to input, and the locations within the network for adding TAM. A key concern is the need to strike an optimal balance between performance and computational efficiency. A comprehensive ablation study was performed by evaluating various configurations for adding TAM to the standard UNet architecture. Table 2 provides a detailed comparison of various configurations (C) outlined in Fig. 2, alongside baseline models: a frame-by-frame UNet2D and an extended UNet3D with a temporal dimension (2D+t).

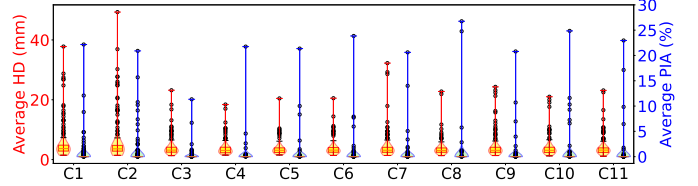


Figure 4: Distribution plots of HD and PIA metrics of different segmentation configurations in Table 2.

Table 2 demonstrates that integrating motion information into UNet2D via our novel TAM leads to a significant improvement ($p \ll 0.05$) across all metrics. In contrast, while UNet3D incorporates motion by adding a temporal dimension to the convolutional layers, it does not outperform the motion-agnostic UNet2D. It significantly worsens the performance in terms of mean HD and PIA and their interquartile ranges (see Fig. 4). Furthermore, employing 3D convolutions (Conv3D) instead of 2D convolutions (Conv2D) markedly increases both FLOPs and trainable parameters, as shown in Table 2. A plausible explanation for this observation is that the evaluation was conducted using only two frames for all methods. Although incorporating additional temporal frames might enhance the performance of conventional motion-based UNet3D [9], it would come at the cost of significantly higher computational complexity. Notably, our TAM-UNet2D achieves superior performance ($p \ll 0.05$) using just two frames (ED and ES) while maintaining computational efficiency, making it a more viable solution for motion-enhanced tasks.

Comparing all TAM configurations (C3–C11), where TAM is integrated into the encoder (\mathcal{E}) and/or decoder (\mathcal{D}), it is evident that the frequency of TAM usage within the network influences FLOPs and trainable parameters. However, the performance is consistent across the various configurations, suggesting a minimal number of TAM modules is needed. Based on Table 2 and the distribution plots of HD and PIA in Fig. 4, configurations C3 and C4 emerge as the optimal TAM-UNet2D designs, achieving optimal performance with minimal computational complexity.

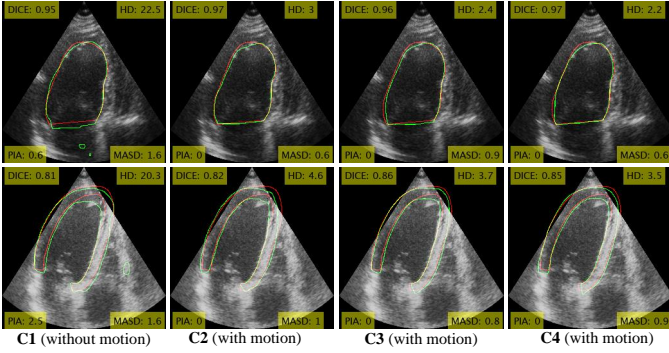


Figure 5: The improvement in segmentation quality is attributed to the incorporation of motion, with the cost-efficient C3 and C4 configurations outperforming the computationally intensive C2 setup.

While the HD and PIA distributions for C3 are balanced, C4 demonstrates a superior HD distribution and a denser PIA distribution, barring a single outlier (see Fig. 4). Compared to the baseline models without TAM (C1 and C2) (Fig. 5 and Table 2), C3 and C4 provided better DSC, HD, MASD, and PIA. They also require much lower FLOPs and have much fewer trainable parameters than the 3D (2D+t) option (C2), suggesting that they are better ways for motion enhancement. Due to their optimality, C3 and C4 are used for subsequent ablation studies focusing on a number of heads and time frames.

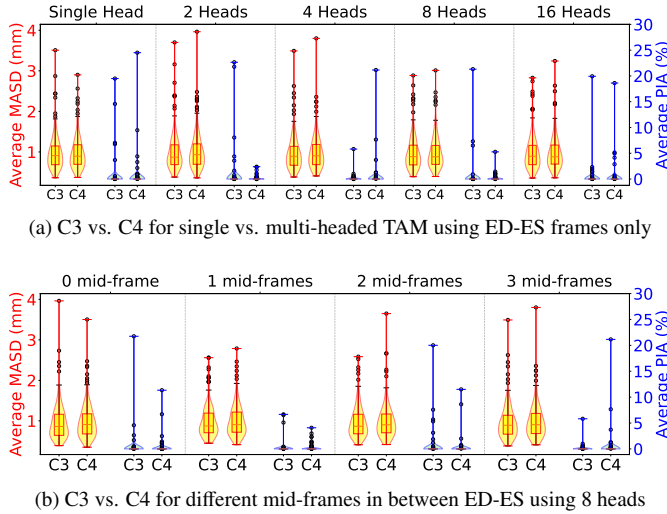


Figure 6: Distribution plots of HD and PIA metrics for our novel TAM-UNet2D configurations (C3 vs. C4) from Table 2, illustrating the impact of single-headed versus multi-headed TAM configurations across varying numbers of mid-frames sampled between the ED and ES frames.

In Fig. 6, we compare the performance of configurations with different numbers of attention heads and time frames. Fig. 6(a) shows that multi-head TAM performed better in MASD and PIA than single-head TAM for both C3 and C4 configurations. As explained above, this is likely because the multi-head approach allows learning of more aspects of images. The 8-headed C4 TAM-UNet is found to be the optimal configuration. In terms of number of input time frames, having mid-frames in between end-diastole and end-systole is found to perform better

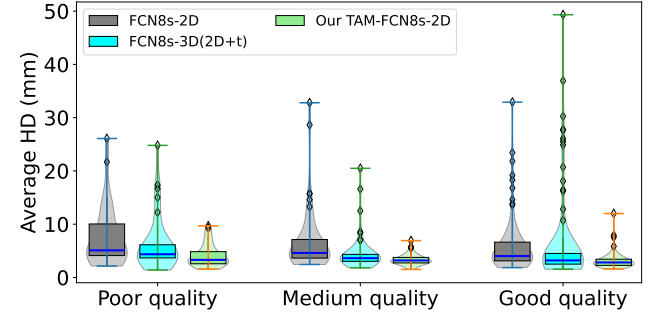


Figure 7: Performance comparison of our motion-aware segmentation model with other models using the same FCN8s backbone architecture across varying image quality levels.

than just inputting end-diastole and end-systole frames into the network (Fig. 6 (b)). This may be because there is too much dissimilarity between the end-diastole and end-systole images in echocardiography, and intermediate frames can help the network understand how to bridge the dissimilarity. The optimal configuration is C4 with one intermediate frame.

Our design of the TAM module is to use the multi-head KQV projection. An alternative design is to compute an attention map between features of various image pairs at the bottleneck layer for multiplication with the original features, such as that proposed by [29, 46] (we name this the vanilla TAM here). We compare the performance of vanilla TAM to our KQV TAM, using the C4 configuration, keeping all hyperparameters constant between the two. Results in Fig. 8 show that HD, MASD, and PIA generally improved with our KQV TAM, with a leftward and upward shift of the cumulative curve and a greater area under the curve. At the same time, the DSC score has similar magnitudes. The figure also demonstrates that both models performed better than UNet without TAM. Our results thus suggest that our design of TAM improves on previous ones.

4.2. TAM integration to CNN and Transformer models

In this section, we investigate the effects of integrating our TAM module into various backbone segmentation networks to enhance them with motion awareness. We study both CNN-based models, such as UNet and FCN8s, and Transformer-based models, such as UNetR and SwinUNetR. The networks are tested on the CAMUS 2D echocardiography dataset, and results are detailed in Table 3. Hyperparameters for each network and TAM are optimized before the investigation.

Results in Table 3 show that the incorporation of TAM consistently improves segmentation performance for all evaluated models, and improvements are statistically significant ($p \ll 0.05$) for most of the cases. Notably, integrating TAM into segmentation models leads to a substantial reduction in HD, indicating improved precision in delineating LV and MYO boundaries. HD improvements are between 23.9% and 48.1%. This improvement is further evident in the qualitative results shown in Fig. 9, where TAM provides more coherent segmentations across the time frames. In contrast, models without TAM produce inconsistent results across time frames. This can lead to poor estimations of clinical parameters such as EF and stroke

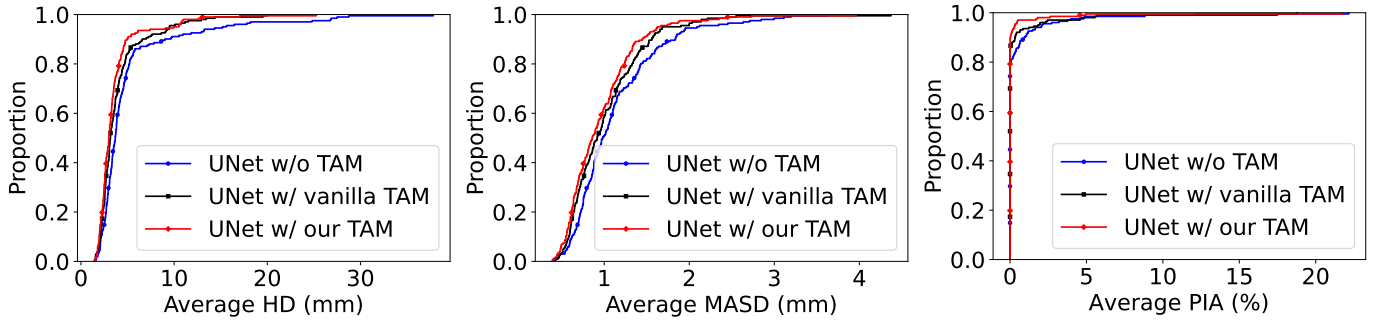


Figure 8: Empirical cumulative distribution curves for the proposed TAM, vanilla TAM, and the model without TAM. The leftward-upper shift indicates a greater proportion of samples achieving smaller error values, highlighting enhanced boundary and surface accuracy.

Table 3: Results of integrating our novel TAM with CNN- and Transformer-based segmentation models using the public CAMUS dataset [11]. The improvements introduced by the TAM are highlighted in bold, while the overall best metrics are colored blue.

Methods	Class-wise HD (mm) (↓)				The average of the anatomical organs			
	LV _{MYO}	LV _{ENDO}	LV _{EPI}	LA	DSC (↑)	HD (mm) (↓)	MASD (mm) (↓)	PIA (%) (↓)
UNet	5.65 ± 7.57	4.21 ± 4.72	5.67 ± 8.12	4.91 ± 8.12	0.913 ± 0.037	5.11 ± 5.14	1.13 ± 0.54	2.05 ± 3.97
TAM-UNet	4.05 ± 3.99	3.07 ± 2.62	3.89 ± 4.40	3.52 ± 4.40	0.922 ± 0.033	3.63 ± 2.69	0.96 ± 0.42	0.68 ± 1.51
FCN8s	6.80 ± 6.82	5.44 ± 4.24	6.01 ± 6.26	7.26 ± 6.26	0.899 ± 0.045	6.38 ± 5.24	1.33 ± 0.78	0.58 ± 1.13
TAM-FCN8s	3.60 ± 1.67	3.04 ± 1.95	3.33 ± 1.86	3.27 ± 1.86	0.921 ± 0.026	3.31 ± 1.47	0.98 ± 0.40	0.02 ± 0.02
UNetR	8.03 ± 8.07	5.59 ± 5.99	7.71 ± 8.17	8.35 ± 8.17	0.897 ± 0.040	7.42 ± 6.65	1.43 ± 0.82	2.43 ± 4.25
TAM-UNetR	6.08 ± 6.11	4.62 ± 4.74	5.86 ± 6.52	6.05 ± 6.52	0.904 ± 0.040	5.65 ± 4.82	1.24 ± 0.67	0.92 ± 3.32
SwinUNetR	8.33 ± 10.98	5.60 ± 6.92	8.24 ± 11.12	6.41 ± 11.12	0.888 ± 0.048	7.15 ± 7.40	1.52 ± 0.94	2.67 ± 4.17
TAM-SwinUNetR	5.63 ± 7.09	4.25 ± 5.23	5.32 ± 7.16	4.11 ± 7.16	0.913 ± 0.033	4.83 ± 4.81	1.15 ± 0.59	1.32 ± 1.93

volumes [45, 48]. Additionally, TAM effectively reduces PIA, leading to cleaner segmentations with fewer structural inconsistencies (islands or broken-up segmentation mass). This will likely support more straightforward and less erroneous downstream quantification of clinical parameters. There are further improvements to Dice scores with TAM incorporation, but this is more subtle.

To evaluate the integration of TAM under varying image quality conditions, we tested the FCN8 network with and without TAM on the CAMUS dataset, which labels images in terms of their quality, categorizing them as good (35%), medium (46%), and poor (19%) quality [11]. The testing set was carefully selected to ensure a balanced representation across these categories for a comprehensive assessment. Results in Fig. 7 show that FCN8s-3D performs slightly better than FCN8s-2D, likely due to the inclusion of temporal sequences and, thus, motion information. Further, these networks produced slightly poorer HD results with poorer-quality images. In comparison, our motion-aware TAM-FCN8s-2D outperforms both models across all image quality categories in HD results, and it is less affected by the image quality, having similar HD results across image types. This suggests that TAM provides an ability to overcome low image quality via motion awareness. Given that low-quality images are very often encountered clinically, this

characteristic is very advantageous.

Overall, our results consistently suggest that TAM can enhance various segmentation networks with the introduction of motion awareness. Improvements in boundary identification and reducing structural abnormalities are especially evident, and TAM is more resistant to image quality issues. TAM’s lightweight design also ensures easy integration and provides computational efficiency.

4.3. TAM’s scalability and cross-dataset genericity

On top of adding TAM to networks performing 2D echocardiography segmentation (Table 3), we further tested the addition of TAM to networks performing 3D segmentation, results of which are shown in Table 4. Here, networks are tested on the MITEA 3D echocardiography dataset. Results in the table again show that TAM consistently delivers significant improvements ($p \ll 0.05$) across various backbone architectures. Our results thus show that TAM is scalable from 2D to 3D segmentation and can successfully enhance motion awareness even with increased image dimensionality.

In both 2D and 3D experiments, TAM enhances segmentation precision across critical metrics such as DSC, HD, and PIA. For instance, in 2D segmentation (Table 3), TAM increases DSC by 1%–2.4%, reduces HD by 14.5%–29%, and

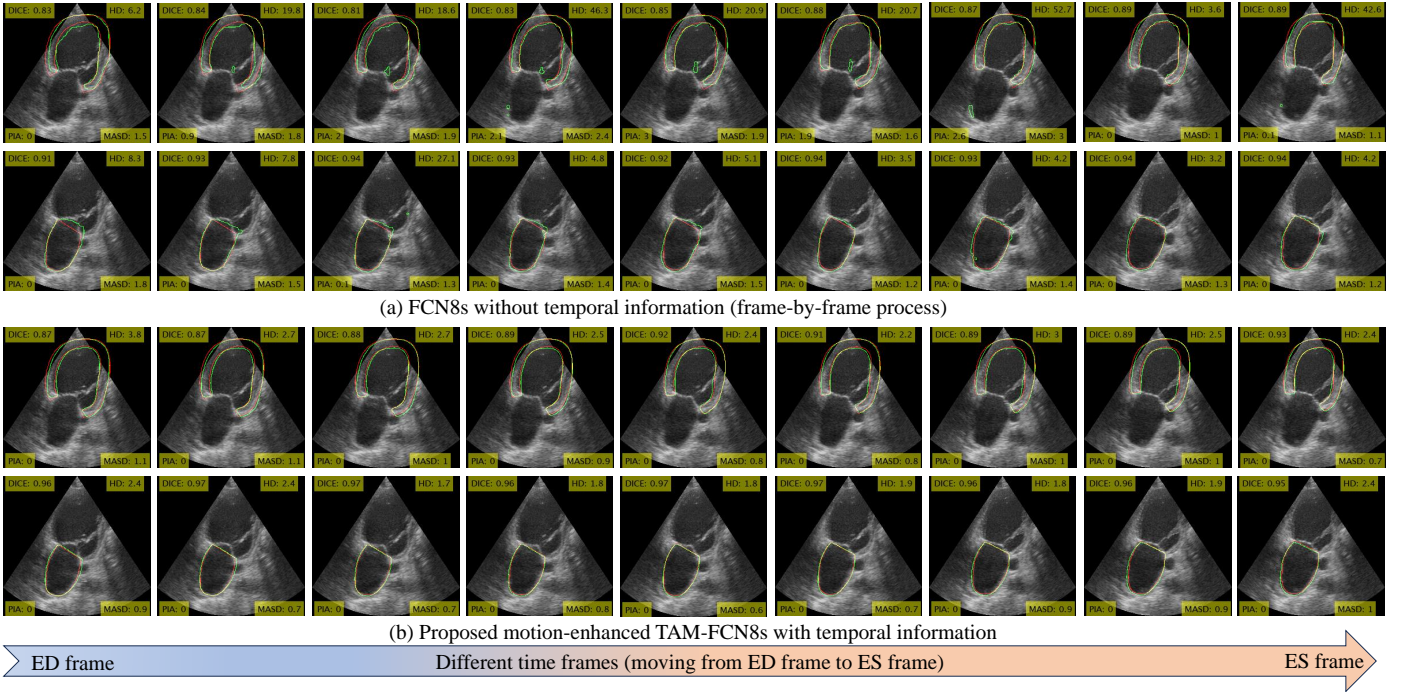


Figure 9: Assessing the temporal consistency of segmentation results using FCN8s, both without motion and with motion integrated through our novel TAM, on the publicly available CAMUS dataset.

Table 4: Results of integrating our novel 3D-TAM with 3D-CNN- and Transformer-based segmentation models using public 3D echocardiography [13]. Improvements introduced by the TAM are highlighted in bold, while the overall best metrics are colored blue.

Methods	Class-wise HD (mm) (↓)				The average of the anatomical organs			
	LV _{MYO}	LV _{ENDO}	LV _{EPI}	LA	DSC (↑)	HD (mm) (↓)	MASD (mm) (↓)	PIA (%) (↓)
UNet	14.58 ± 8.65	9.89 ± 6.84	12.31 ± 9.31	–	0.830 ± 0.045	12.26 ± 7.25	2.03 ± 0.54	0.30 ± 0.50
TAM-UNet	11.47 ± 8.40	9.14 ± 6.67	10.84 ± 8.65	–	0.833 ± 0.045	10.48 ± 6.90	1.97 ± 0.48	0.16 ± 0.19
FCN8s	12.07 ± 7.91	11.95 ± 5.80	10.95 ± 8.06	–	0.828 ± 0.046	11.66 ± 6.55	2.06 ± 0.57	1.07 ± 1.04
TAM-FCN8s	9.27 ± 5.10	7.59 ± 2.05	8.24 ± 5.14	–	0.836 ± 0.043	8.37 ± 3.75	1.93 ± 0.55	0.22 ± 0.30
UNetR	13.39 ± 9.45	11.85 ± 9.48	12.74 ± 9.65	–	0.806 ± 0.052	12.66 ± 9.10	2.34 ± 0.79	0.53 ± 0.88
TAM-UNetR	10.70 ± 6.88	9.56 ± 5.93	9.96 ± 7.01	–	0.814 ± 0.058	10.07 ± 6.40	2.21 ± 0.08	0.38 ± 0.61
SwinUNetR	10.95 ± 7.30	10.10 ± 7.98	10.25 ± 7.85	–	0.818 ± 0.058	10.43 ± 7.63	2.27 ± 1.11	0.36 ± 0.63
TAM-SwinUNetR	9.67 ± 5.38	8.67 ± 6.13	9.01 ± 5.83	–	0.823 ± 0.049	9.12 ± 5.67	2.12 ± 0.78	0.23 ± 0.44

decreases PIA by 46.7%–96.6%. Similarly, in 3D segmentation (Table 4), TAM improves DSC by 0.6%–1.7%, reduces HD by 12.6%–28.2%, and decreases PIA by 46.7%–91.3%. These consistent gains highlight TAM’s scalability to higher-dimensional data. Despite higher computational burden and complexity, TAM offers similar improvements in 3D images compared to 2D images. Compared to 2D images, 3D images face additional anatomical complexity, a sparser percentage region of interest, and are more challenging to segment. Our results in tables 3 and 4 corroborate this notion. Having TAM temporal awareness to enhance performance is thus useful.

TAM’s cross-backbone performance further highlights its versatility. In 2D tasks, it achieves its highest DSC gains for

FCN8s (from 0.899 to 0.921) and SwinUNetR (from 0.888 to 0.913). In 3D tasks, TAM achieves substantial HD reductions, particularly for CNN-based models like FCN8s (from 11.66 mm to 8.37 mm) and SwinUNetR (from 10.43 mm to 9.12 mm). While transformer-based models, such as SwinUNetR, start with superior baseline DSC values, TAM provides more pronounced relative improvements for CNN-based models, particularly in reducing HD and PIA. These results highlight TAM’s adaptability to diverse architectural designs, making it a valuable addition to CNN and transformer backbones.

Beyond these quantitative gains, TAM demonstrates remarkable robustness to dataset-specific challenges. For example, in CAMUS-2D (Table 3), TAM reduces HD for UNet from 5.11

Table 5: Comparison of segmentation performance on the CAMUS dataset across state-of-the-art methods and our proposed motion-aware TAM-based segmentation models. Best-performing metrics are highlighted in bold blue.

Methods (motion?)	LV _{MYO}			LV _{ENDO}			LV _{EPI}			LA		
	DSC (↑)	HD (↓)	MASD (↓)	DSC (↑)	HD (↓)	MASD (↓)	DSC (↑)	HD (↓)	MASD (↓)	DSC (↑)	HD (↓)	MASD (↓)
UNet [17] (✗)	0.864	5.65	1.10	0.927	4.21	1.06	0.954	5.67	1.15	0.904	4.91	1.21
SwinUNetR [23] (✗)	0.834	8.33	1.41	0.908	5.60	1.42	0.939	8.24	1.56	0.869	6.41	1.68
ACNN [49] (✗)	–	–	–	0.918	5.90	1.80	0.946	6.35	1.95	–	–	–
BEASNet [50] (✗)	–	–	–	0.915	6.0	1.95	0.943	6.35	2.15	–	–	–
UB ² DNet [51] (✗)	–	–	–	0.858	–	–	–	–	–	–	–	–
FFPN-R [52] (✗)	0.850	3.65	–	0.924	3.05	–	–	–	–	0.888	3.80	–
PLANNet [53] (✗)	–	–	–	0.944	4.14	1.26	0.957	5.0	1.72	–	–	–
CoST-UNet [54] (✗)	–	–	–	0.916	6.55	–	0.837	7.65	–	0.875	6.70	–
I ² UNet [30] (✗)	0.873	4.72	1.03	0.933	3.49	1.02	0.956	4.39	1.09	0.910	4.25	1.19
TAM-I²UNet (✓)	0.872	4.19	1.03	0.933	3.02	0.972	0.956	3.92	1.06	0.913	3.74	1.11
SOCOF [25] (✓)	–	–	–	0.932	3.21	1.40	0.953	4.0	1.65	–	–	–
CLAS [9] (✓)	–	–	–	0.935	4.60	1.40	0.958	4.85	1.55	0.915	5.0	1.85
TAM-FCN8s (✓)	0.876	3.60	0.973	0.935	3.04	0.949	0.959	3.33	0.961	0.916	3.27	1.06

mm to 3.63 mm and nearly eliminates PIA for FCN8s (from 0.58% – 0.02%). Similarly, in MITEA-3D (Table 4), TAM achieves comparable reductions in HD (e.g., from 12.26 mm to 10.48 mm for UNet) and PIA (e.g., from 1.07% – 0.22% for FCN8s). These results indicate TAM’s ability to dynamically focus on relevant spatial-temporal features, which applies to diverse datasets with different image quality variability, cardiac views, temporal coverage, and resolution. It is thus a generalizability.

Finally, TAM’s ability to reduce PIA to near-zero levels in 2D (e.g., from 0.58% – 0.02% for FCN8s) and significantly in 3D (e.g., from 1.07% – 0.22% for FCN8s) highlights its capacity to minimize incorrect segmentation regions. This has direct implications for improving the reliability of automated cardiac assessments, particularly in edge cases involving poor image quality or challenging anatomical features. Overall, our results suggest that TAM is easily scalable to 3D, is as easy to implement in 3D as in 2D, and offers consistent improvements in 2D and 3D tasks. Results also show that TAM is generalizable, performing similarly well in two different datasets.

4.4. Comparison to SOTA

In Table 5, we compare our optimal TAM configuration, the TAM-FCN8s, to several prominent and high-performing 2D echocardiography segmentation models to demonstrate that TAM can enable SOTA advancement. We compared segmentation of the left ventricular myocardium, endocardial and epicardial boundary, and the left atrial endocardial boundaries in terms of DSC, HD, and MASD. Results show that TAM-FCN8s has the best overall performance, with the best metrics for the left ventricular myocardium, epicardium, and left atrium.

In our analysis, we included the I2UNet, which encourages historical information reuse and re-exploration through rich information interaction among the dual paths. This allows deep layers to learn more comprehensive features that contain both low-level detail description and high-level semantic abstraction and is arguably a SOTA. This recent network has been tested

with the addition of our novel TAM. This I²UNet produced very good DSC, HD, and MASD. We observe that TAM did not significantly improve its DSC score, but it significantly ($p \ll 0.05$) improved HD at all anatomical regions. This further proves TAM’s ability to improve modern, cutting-edge models and its utility as a plug-and-play motion awareness enhancer.

Compared to high-performance motion-aware methods like SOCOF and CLAS, TAM-FCN8s produced similar DSC but improved HD and MASD substantially. SOCOF relies on optical flow to extract motion dynamics [25], while CLAS performs concurrent DL registration and segmentation [9]. TAM has a much lighter architecture than these networks, as it requires only three frames as inputs instead of the entire cardiac cycle, and it has a comparatively simple network with a low number of trainable parameters. Despite this, it can provide sufficient motion awareness to the simple FCN network to match and improve complex motion-enhanced methods. This demonstrates TAM’s robust performance.

5. Discussions and Conclusion

Past studies [9, 25, 28, 29, 46] have demonstrated that providing an awareness of temporal motions can improve echocardiography segmentation, likely because it can utilize neighboring time frames to mitigate difficulties posed by localized, transient noise and signal losses and because coherent features across different time frames can aid in more accurate delineation of anatomic boundaries. We proposed a novel approach to enabling motion awareness in segmentation networks via the TAM module, which can be inserted into various networks for enhancement.

TAM’s uniqueness is in its plug-and-play approach. Having an adaptable design, it can be easily inserted at various locations of both CNN- and transformer-based networks, and having a small and simple architecture, it does not impose substantial additional computational burden and risk of overfitting on

the network and does not impede the original network’s training. As an adaptable module rather than a standalone framework, TAM will likely be easily incorporated in future segmentation implementations, enabling easy and convenient inclusion of motion awareness. A second innovation is that TAM uses the multi-head KQV projection as the attention mechanism instead of computing a co-attention map [29, 46]. Our experiments show that this enables performance improvements.

TAM further has other advantages. First, it does not require a substantial increase in input data size, as it only needs about three images for motion enhancement. This avoids excessive computational burden and allows flexibility in deciding which time points to focus on. It also allows effective network training when only a few sparse frames of image labels are available. Second, our test results show that it provides improvements to segmentation performance.

Our results, summarized in Tables 3, 4, and 5, demonstrate TAM’s consistent enhancement across different model architectures. While it has only a mild ability to improve DICE, TAM significantly reduces HD and MASD, suggesting that it delineates boundaries with greater precision. TAM also significantly reduces PIA and enables much better mitigation to the frequently encountered problems of segmentation island and broken-up segmentation masses, offering cleaner and more coherent segmentations across time frames. These advantages may offer accuracy and precision in clinical parameter quantifications after segmentation.

Declaration of Competing Interest

The authors declare that they have no known competing financial interests or personal relationships that could have appeared to influence the work reported in this paper.

Acknowledgement

M. K. Hasan was supported by the EPSRC-DTP studentship funds (2022-2026) from the Bioengineering department of Imperial College London, UK.

G. Yang was supported in part by the ERC IMI (101005122), the H2020 (952172), the MRC (MC/PC/21013), the Royal Society (IEC/NSFC/211235), the NVIDIA Academic Hardware Grant Program, the SABER project supported by Boehringer Ingelheim Ltd, NIHR Imperial Biomedical Research Centre (RDA01), Wellcome Leap Dynamic Resilience, UKRI guarantee funding for Horizon Europe MSCA Postdoctoral Fellowships (EP/Z002206/1), and the UKRI Future Leaders Fellowship (MR/V023799/1).

References

- [1] W. Bai, M. Sinclair, G. Tarroni, O. Oktay, M. Rajchl, G. Vaillant, A. M. Lee, N. Aung, E. Lukaschuk, M. M. Sanghvi, et al., Automated cardiovascular magnetic resonance image analysis with fully convolutional networks, *Journal of cardiovascular magnetic resonance* 20 (2018) 65.
- [2] C. Petitjean, J.-N. Dacher, A review of segmentation methods in short axis cardiac mr images, *Medical image analysis* 15 (2011) 169–184.
- [3] P. A. Heidenreich, J. G. Trogdon, O. A. Khavjou, J. Butler, K. Dracup, M. D. Ezekowitz, E. A. Finkelstein, Y. Hong, S. C. Johnston, A. Khera, et al., Forecasting the future of cardiovascular disease in the united states: a policy statement from the american heart association, *Circulation* 123 (2011) 933–944.
- [4] R. Adams, L. Bischof, Seeded region growing, *IEEE Transactions on pattern analysis and machine intelligence* 16 (1994) 641–647.
- [5] W. Chen, R. Smith, S.-Y. Ji, K. R. Ward, K. Najarian, Automated ventricular systems segmentation in brain ct images by combining low-level segmentation and high-level template matching, *BMC medical informatics and decision making* 9 (2009) 1–14.
- [6] C. Li, X. Wang, S. Eberl, M. Fulham, Y. Yin, J. Chen, D. D. Feng, A likelihood and local constraint level set model for liver tumor segmentation from ct volumes, *IEEE Transactions on Biomedical Engineering* 60 (2013) 2967–2977.
- [7] J. Li, N. Chen, H. Zhou, T. Lai, H. Dong, C. Feng, R. Chen, C. Yang, F. Cai, L. Wei, Mrformer: Morphological constraint reticular transformer for 3d medical image segmentation, *Expert Systems with Applications* 232 (2023) 120877.
- [8] R. M. Lang, L. P. Badano, V. Mor-Avi, J. Afilalo, A. Armstrong, L. Ernande, F. A. Flachskampf, E. Foster, S. A. Goldstein, T. Kuznetsova, et al., Recommendations for cardiac chamber quantification by echocardiography in adults: an update from the american society of echocardiography and the european association of cardiovascular imaging, *European Heart Journal-Cardiovascular Imaging* 16 (2015) 233–271.
- [9] H. Wei, H. Cao, Y. Zhou, W. Xue, D. Ni, S. Li, Temporal-consistent segmentation of echocardiography with co-learning from appearance and shape, in: *Medical Image Computing and Computer Assisted Intervention–MICCAI 2020: 23rd International Conference, Lima, Peru, October 4–8, 2020, Proceedings, Part II* 23, Springer, pp. 623–632.
- [10] A. Myronenko, D. Yang, V. Buch, D. Xu, A. Ihsani, S. Doyle, M. Michalski, N. Tenenholtz, H. Roth, 4d cnn for semantic segmentation of cardiac volumetric sequences, in: *Statistical Atlases and Computational Models of the Heart. Multi-Sequence CMR Segmentation, CRT-EPiggy and LV Full Quantification Challenges: 10th International Workshop, STACOM 2019, Held in Conjunction with MICCAI 2019, Shenzhen, China, October 13, 2019, Revised Selected Papers* 10, Springer, pp. 72–80.
- [11] S. Leclerc, E. Smistad, J. Pedrosa, A. Østvik, F. Cervenansky, F. Espinosa, T. Espeland, E. A. R. Berg, P.-M. Jodoin, T. Grenier, et al., Deep learning for segmentation using an open large-scale dataset in 2d echocardiography, *IEEE transactions on medical imaging* 38 (2019) 2198–2210.
- [12] D. Ouyang, B. He, A. Ghorbani, N. Yuan, J. Ebinger, C. P. Langlotz, P. A. Heidenreich, R. A. Harrington, D. H. Liang, E. A. Ashley, et al., Video-based ai for beat-to-beat assessment of cardiac function, *Nature* 580 (2020) 252–256.
- [13] D. Zhao, E. Ferdinand, G. D. Maso Talou, G. M. Quill, K. Gilbert, V. Y. Wang, T. P. Babarenda Gamage, J. Pedrosa, J. D’hooge, T. M. Sutton, et al., Mitea: A dataset for machine learning segmentation of the left ventricle in 3d echocardiography using subject-specific labels from cardiac magnetic resonance imaging, *Frontiers in Cardiovascular Medicine* 9 (2023) 1016703.
- [14] O. Bernard, A. Lalande, C. Zotti, F. Cervenansky, X. Yang, P.-A. Heng, I. Cetin, K. Lekadir, O. Camara, M. A. G. Ballester, et al., Deep learning techniques for automatic mri cardiac multi-structures segmentation and diagnosis: is the problem solved?, *IEEE transactions on medical imaging* 37 (2018) 2514–2525.
- [15] G. Litjens, T. Kooi, B. E. Bejnordi, A. A. A. Setio, F. Ciompi, M. Ghafoorian, J. A. Van Der Laak, B. Van Ginneken, C. I. Sánchez, A survey on deep learning in medical image analysis, *Medical image analysis* 42 (2017) 60–88.
- [16] J. Long, E. Shelhamer, T. Darrell, Fully convolutional networks for semantic segmentation, in: *Proceedings of the IEEE conference on computer vision and pattern recognition*, pp. 3431–3440.
- [17] O. Ronneberger, P. Fischer, T. Brox, U-net: Convolutional networks for biomedical image segmentation, in: *Medical image computing and computer-assisted intervention–MICCAI 2015: 18th international conference, Munich, Germany, October 5–9, 2015, proceedings, part III* 18, Springer, pp. 234–241.
- [18] K. Han, Y. Wang, H. Chen, X. Chen, J. Guo, Z. Liu, Y. Tang, A. Xiao, C. Xu, Y. Xu, et al., A survey on vision transformer, *IEEE transactions on pattern analysis and machine intelligence* 45 (2022) 87–110.

[19] J. Chen, Y. Lu, Q. Yu, X. Luo, E. Adeli, Y. Wang, L. Lu, A. L. Yuille, Y. Zhou, Transunet: Transformers make strong encoders for medical image segmentation, arXiv:2102.04306 (2021).

[20] G. Xu, X. Zhang, X. He, X. Wu, Levit-unet: Make faster encoders with transformer for medical image segmentation, in: Chinese Conference on Pattern Recognition and Computer Vision (PRCV), Springer, pp. 42–53.

[21] H. Yang, D. Yang, Cswin-pnnet: A cnn-swin transformer combined pyramid network for breast lesion segmentation in ultrasound images, *Expert Systems with Applications* 213 (2023) 119024.

[22] A. Hatamizadeh et al., Unetr: Transformers for 3d medical image segmentation, in: Proceedings of the IEEE/CVF winter conference on applications of computer vision, pp. 574–584.

[23] A. Hatamizadeh, et al., Swin unetr: Swin transformers for semantic segmentation of brain tumors in mri images, in: International MICCAI Brainlesion Workshop, Springer, pp. 272–284.

[24] W. X. Chan, Y. Zheng, H. Wiputra, H. L. Leo, C. H. Yap, Full cardiac cycle asynchronous temporal compounding of 3d echocardiography images, *Medical Image Analysis* 74 (2021) 102229.

[25] W. Xue, H. Cao, J. Ma, T. Bai, T. Wang, D. Ni, Improved segmentation of echocardiography with orientation-congruency of optical flow and motion-enhanced segmentation, *IEEE Journal of Biomedical and Health Informatics* 26 (2022) 6105–6115.

[26] M. Li, W. Zhang, G. Yang, C. Wang, H. Zhang, H. Liu, W. Zheng, S. Li, Recurrent aggregation learning for multi-view echocardiographic sequences segmentation, in: Medical Image Computing and Computer Assisted Intervention—MICCAI 2019: 22nd International Conference, Shenzhen, China, October 13–17, 2019, Proceedings, Part II 22, Springer, pp. 678–686.

[27] H. Wu, J. Liu, F. Xiao, Z. Wen, L. Cheng, J. Qin, Semi-supervised segmentation of echocardiography videos via noise-resilient spatiotemporal semantic calibration and fusion, *Medical Image Analysis* 78 (2022) 102397.

[28] H. Wei, J. Ma, Y. Zhou, W. Xue, D. Ni, Co-learning of appearance and shape for precise ejection fraction estimation from echocardiographic sequences, *Medical Image Analysis* 84 (2023) 102686.

[29] S. S. Ahn, K. Ta, S. Thorn, J. Langdon, A. J. Sinusas, J. S. Duncan, Multi-frame attention network for left ventricle segmentation in 3d echocardiography, in: Medical Image Computing and Computer Assisted Intervention—MICCAI 2021: 24th International Conference, Strasbourg, France, September 27–October 1, 2021, Proceedings, Part I 24, Springer, pp. 348–357.

[30] D. Dai, C. Dong, Q. Yan, Y. Sun, C. Zhang, Z. Li, S. Xu, I2u-net: A dual-path u-net with rich information interaction for medical image segmentation, *Medical Image Analysis* (2024) 103241.

[31] F. Isensee, P. F. Jaeger, S. A. Kohl, J. Petersen, K. H. Maier-Hein, nnunet: a self-configuring method for deep learning-based biomedical image segmentation, *Nature methods* 18 (2021) 203–211.

[32] M. K. Hasan, M. A. Alam, M. T. E. Elahi, S. Roy, R. Martí, Drnet: Segmentation and localization of optic disc and fovea from diabetic retinopathy image, *Artificial Intelligence in Medicine* 111 (2021) 102001.

[33] Z. Zhou, M. M. Rahman Siddiquee, N. Tajbakhsh, J. Liang, Unet++: A nested u-net architecture for medical image segmentation, in: Deep Learning in Medical Image Analysis and Multimodal Learning for Clinical Decision Support: 4th International Workshop, DLMIA 2018, and 8th International Workshop, ML-CDS 2018, Held in Conjunction with MICCAI 2018, Granada, Spain, September 20, 2018, Proceedings 4, Springer, pp. 3–11.

[34] Ö. Çiçek, A. Abdulkadir, S. S. Lienkamp, T. Brox, O. Ronneberger, 3d u-net: learning dense volumetric segmentation from sparse annotation, in: Medical Image Computing and Computer-Assisted Intervention—MICCAI 2016: 19th International Conference, Athens, Greece, October 17–21, 2016, Proceedings, Part II 19, Springer, pp. 424–432.

[35] H. Zhao, J. Shi, X. Qi, X. Wang, J. Jia, Pyramid scene parsing network, in: Proceedings of the IEEE conference on computer vision and pattern recognition, pp. 2881–2890.

[36] C. Peng, X. Zhang, G. Yu, G. Luo, J. Sun, Large kernel matters—improve semantic segmentation by global convolutional network, in: Proceedings of the IEEE conference on computer vision and pattern recognition, pp. 4353–4361.

[37] L.-C. Chen, Y. Zhu, G. Papandreou, F. Schroff, H. Adam, Encoder-decoder with atrous separable convolution for semantic image segmentation, in: Proceedings of the European conference on computer vision (ECCV), pp. 801–818.

[38] Z. Li, H. Pan, Y. Zhu, A. K. Qin, PgD-unet: A position-guided deformable network for simultaneous segmentation of organs and tumors, in: 2020 International Joint Conference on Neural Networks (IJCNN), IEEE, pp. 1–8.

[39] H.-Y. Zhou, J. Guo, Y. Zhang, X. Han, L. Yu, L. Wang, Y. Yu, nnformer: Volumetric medical image segmentation via a 3d transformer, *IEEE Transactions on Image Processing* (2023).

[40] Y. Zhao, K. Liao, Y. Zheng, X. Zhou, X. Guo, Boundary attention with multi-task consistency constraints for semi-supervised 2d echocardiography segmentation, *Computers in Biology and Medicine* 171 (2024) 108100.

[41] D. Zhang, C. Lu, T. Tan, B. Dashtbozorg, X. Long, X. Xu, J. Zhang, C. Shan, Bsanet: Boundary-aware and scale-aggregation networks for cmr image segmentation, *Neurocomputing* 599 (2024) 128125.

[42] A. M. Shaker, M. Maaz, H. Rasheed, S. Khan, M.-H. Yang, F. S. Khan, Unetr++: delving into efficient and accurate 3d medical image segmentation, *IEEE Transactions on Medical Imaging* (2024).

[43] C. Qin, Y. Wang, J. Zhang, Urca: Uncertainty-based region clipping algorithm for semi-supervised medical image segmentation, *Computer Methods and Programs in Biomedicine* (2024) 108278.

[44] Z. Li, J. Zhang, S. Wei, Y. Gao, C. Cao, Z. Wu, Tpafnet: Transformer-driven pyramid attention fusion network for 3d medical image segmentation, *IEEE Journal of Biomedical and Health Informatics* (2024).

[45] F. Maani, A. Ukyay, N. Saadi, N. Saeed, M. Yaqub, Simlvseg: Simplifying left ventricular segmentation in 2-d+ time echocardiograms with self- and weakly supervised learning, *Ultrasound in Medicine & Biology* (2024).

[46] X. Lu, W. Wang, C. Ma, J. Shen, L. Shao, F. Porikli, See more, know more: Unsupervised video object segmentation with co-attention siamese networks, in: Proceedings of the IEEE/CVF conference on computer vision and pattern recognition, pp. 3623–3632.

[47] A. M. Shaker, M. Maaz, H. Rasheed, S. Khan, M.-H. Yang, F. S. Khan, Unetr++: delving into efficient and accurate 3d medical image segmentation, *IEEE Transactions on Medical Imaging* (2024).

[48] A. A. Amadou, Y. Zhang, S. Piat, P. Klein, I. Schmuëcking, T. Passerini, P. Sharma, Echoapex: A general-purpose vision foundation model for echocardiography, arXiv:2410.11092 (2024).

[49] O. Oktay, E. Ferrante, K. Kamnitsas, M. Heinrich, W. Bai, J. Caballero, S. A. Cook, A. De Marvao, T. Dawes, D. P. O'Regan, et al., Anatomically constrained neural networks (acnns): application to cardiac image enhancement and segmentation, *IEEE transactions on medical imaging* 37 (2017) 384–395.

[50] S. Akbari, M. Tabassian, J. Pedrosa, S. Queirós, K. Papangelopoulou, J. D'hooge, Beas-net: a shape-prior-based deep convolutional neural network for robust left ventricular segmentation in 2d echocardiography, *IEEE Transactions on Ultrasonics, Ferroelectrics, and Frequency Control* (2024).

[51] X. Cui, B. Wang, S. Jiang, Z. Liu, H. Xu, L. Cui, S. Li, Unified bi-encoder bispace-discriminator disentanglement for cross-domain echocardiography segmentation, *Knowledge-Based Systems* 303 (2024) 112394.

[52] C. Chen, X. Yang, R. Chen, J. Yu, L. Du, J. Wang, X. Hu, Y. Cao, Y. Liu, D. Ni, Ffpn: Fourier feature pyramid network for ultrasound image segmentation, in: International Workshop on Machine Learning in Medical Imaging, Springer, pp. 166–175.

[53] F. Liu, K. Wang, D. Liu, X. Yang, J. Tian, Deep pyramid local attention neural network for cardiac structure segmentation in two-dimensional echocardiography, *Medical image analysis* 67 (2021) 101873.

[54] M. R. Islam, M. Qaraqe, E. Serpedin, Cost-unet: Convolution and swin transformer based deep learning architecture for cardiac segmentation, *Biomedical Signal Processing and Control* 96 (2024) 106633.